Computational Cross-Validation of Propeller Noise in Positive and Negative Thrust Conditions

Wickersheim, Robin ; Goyal, J.; Sinnige, T.; Keßle, Manuel

DOI
10.2514/6.2025-1046

Publication date
2025

Document Version
Final published version

Published in
Proceedings of the AIAA SCITECH 2025 Forum

AIAA SciTech Forum
6-10 January 2025, Orlando, FL
AIAA SCITECH 2025 Forum

10.2514/6.2025-1046

Computational Cross-Validation of Propeller Noise in Positive and Negative Thrust Conditions

Robin Wickersheim[*,a], Jatinder Goyal[†,b], Tomas Sinnige[‡,b], and Manuel Keßler[§,a]
[a] *University of Stuttgart, Institute of Aerodynamics and Gas Dynamics, 70563 Stuttgart, Germany*
[b] *Delft University of Technology, Kluyverweg 1, Delft 2629 HS, The Netherlands*

This study deals with the comparison of different numerical fidelity levels to predict the noise of an isolated propeller in positive and negative thrust conditions. For this purpose, unsteady Reynolds-Averaged Navier-Stokes (URANS) and Improved Delayed Detached-Eddy Simulations (IDDES) were carried out and compared with Lattice Boltzmann (LBM) very large eddy simulations and wind tunnel data measured at TU Delft. It was found that the aerodynamic behavior with respect to the propeller loads, flow field in the slipstream, and surface pressure was well predicted by all methods. In the subsequent acoustic propagation, according to the Ffowcs Williams - Hawkings analogy, it was found that the noise directivity differed when using different CFD methods for the case of negative thrust due to increased broadband noise, while all CFD methods showed a similar noise directivity at the first blade passing frequency in the positive thrust condition. In the negative regime, the URANS simulation did not take into account the broadband fluctuations, which led to a significant underestimation of about 40 dB **in streamwise directions in the overall noise, while IDDES and LBM showed similar trends, but still deviated about** 5 dB **in the prediction of the overall noise. Finally, a study was conducted with a low-fidelity acoustic evaluation based on Hanson's model, which enabled a direct comparison of noise generated only by propeller loads, where a good agreement in tonal noise was achieved compared to the FW-H formulation with all CFD methods exhibit a similar noise directivity in both operation conditions.**

Nomenclature

B	=	number of propeller blades, [-]	P	=	propeller power, [W]
BPF	=	$B \cdot n$, blade passing frequency, [Hz]	q_∞	=	$\rho V_\infty^2/2$, dynamic pressure [Pa]
c	=	section chord, [m]	q_{eff}	=	$\rho V_\infty^2/2 + (\Omega r)^2$, effective dynamic pressure, [Pa]
c_{P}	=	$(p - p_\infty)/q_{\text{eff}}$, pressure coefficient, [-]	Q	=	propeller torque, [Nm]
$c_{\text{P,tot}}$	=	$(p_t - p_\infty)/q_\infty$, total pressure coefficient, [-]	r	=	radial coordinate, [m]
C_{T}	=	$T/\rho_\infty n^2 D^4$, propeller thrust coefficient, [-]	R	=	propeller radius, [m]
C_{P}	=	$P/\rho_\infty n^3 D^5$, propeller power coefficient, [-]	s	=	cell size, [m]
D	=	propeller diameter, [m]	T	=	propeller thrust, [N]
f	=	frequency, [Hz]	V_∞	=	free-stream velocity, [m/s]
J	=	V_∞/nD, advance ratio, [-]	x, y, z	=	coordinates, [m/s]
L_{P}	=	sound pressure level, [dB]	η_P	=	TV_∞/P, propeller efficiency, [-]
n	=	propeller rotation speed, [Hz]	η_t	=	P/TV_∞, turbine efficiency, [-]
N	=	number of grid cells, [-]	Ω	=	$2\pi n$, rotational speed, [rad/s]
p	=	sound pressure, [Pa]	Θ	=	fly-over directivity, [°]
p_{ref}	=	reference sound pressure, 2×10^{-5}Pa	Ψ	=	azimuthal directivity, [°]
p_t	=	total pressure, [Pa]	ρ_∞	=	air density, [kg/m^3]

[*]Research Assistant, Institute of Aerodynamics and Gas Dynamics, Wankelstraße 3; robin.wickersheim@iag.uni-stuttgart.de.
[†]PhD candidate, Wind Energy Section, Faculty of Aerospace Engineering, Kluyverweg 1.
[‡]Assistant Professor, Flight Performance and Propulsion Section, Faculty of Aerospace Engineering, Kluyverweg 1.
[§]Senior Researcher, Institute of Aerodynamics and Gas Dynamics, Member AIAA, Wankelstraße 3.

I. Introduction

The aviation industry aims towards a transition to sustainability, exploring innovative concepts in aircraft propulsion. In this pursuit, the focus is on electrical or hybrid-electric propulsion. One promising concept involves the distribution of multiple smaller propellers across the wing span, replacing conventional main propulsion systems. This approach offers numerous advantages, including lift augmentation through propeller slipstreams and increased flexibility in design layout [1–4]. These advancements have led to the development of beneficial configurations featuring inner-distributed propulsion complemented by a wing-tip-mounted propeller (WTP) [5]. Leveraging such configurations can facilitate reduced landing distances [6], for instance, by utilizing the windmilling condition of the WTP, which is also the scope of future research. Additionally, the generated torque from the WTP or inner propellers can be utilized since the propellers are driven electrically and the electric motors can operate as generators, recuperating energy in descent flight. However, there's ongoing research into mitigating the noise emissions associated with these configurations. Extensive studies incorporating high-fidelity simulation techniques like Lattice-Boltzmann (LBM) very large eddy simulations [7, 8] and experimental measurements [9] have shed light on challenges such as flow separation during specific operational conditions. Additionally, existing literature outlines aeroacoustic behaviors under steady Reynolds-Averaged Navier-Stokes (RANS) and low-fidelity Blade Element Method (BEM) simulations, highlighting their inherent limitations [10, 11]. To close this gap, this work aims to perform a comprehensive aeroacoustic comparison of different numerical methods by conducting unsteady Reynolds-Averaged Navier-Stokes simulations (URANS) and Improved Delayed Detached-Eddy Simulations (IDDES) and comparing them with Lattice Boltzmann (LBM) very large eddy simulations and experimental data from TU Delft. By doing so, it seeks to extend the knowledge of the capabilities from different numerical methods, laying the foundation for future applications, including the integration of propulsive and regenerative propellers within the aforementioned Distributed Electric Propulsion (DEP) configuration.

II. Methodology

A. Setup

The setup comprises the TUD-XPROP, featuring three blades with a diameter of $D = 0.4064\,\mathrm{m}$ and a hub diameter of $D = 0.092\,\mathrm{m}$ [12]. At 70 % of the propeller blade radius, the pitch angle is set to 15 °. The blades are affixed to a spinner, seamlessly integrated into a nacelle extending 1.6 D downstream of the setup. Furthermore, the support structure included in the experiments is omitted to facilitate the simulations. Referencing Figure 1, the setup is visually depicted, showcasing the arrangement alongside the polar angles crucial for acoustic evaluation.

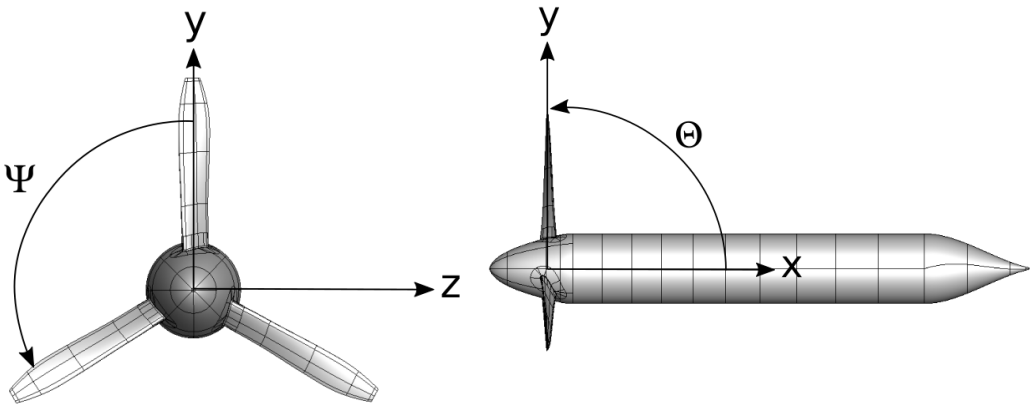

(a) **Front view** (b) **Side view**

Fig. 1 Setup of the XPROP configuration.

Within this study, two operating points are investigated: first, the positive thrust case, characterized by a propeller rotational speed of 123.03 Hz, and second, the negative thrust condition, where the propeller rotational speed was decreased to 67.11 Hz. In both instances, the inflow velocity remains constant at $V_\infty = 30\,\mathrm{m/s}$, with no inclination angle considered, thereby yielding advance ratios of $J = 0.6$ and $J = 1.1$, respectively. Further details on the setup can be

found in the relevant literature [7, 8, 10]. The simulation results are compared to experimental data obtained from wind tunnel tests conducted at TU Delft [9].

B. Numerical Methods

For the unsteady Reynolds-Averaged Navier-Stokes and Improved Delayed Detached-Eddy simulations [13], the finite volume solver FLOWer is applied. Originally developed at the German Aerospace Center (DLR) [14], FLOWer undergoes continuous extension at the Institute of Aerodynamics and Gas Dynamics at the University of Stuttgart [15, 16], with particular applications to rotorcraft [17–20]. For temporal discretization, a second-order dual-time stepping scheme is employed, and a second-order Jameson-Schmidt-Turkel (JST) scheme for spatial discretization. Applying a 5^{th}-order weighted essentially non-oscillatory (WENO) scheme in the background mesh enhances the accurate resolution of the propeller tip vortices [21]. To close the URANS equations, the Menter-SST turbulence model is employed [22]. Similarly, the IDDES simulations utilize the Menter-SST model as the underlying turbulence model, comprehensively analyzed in various studies employing FLOWer [23, 24]. FLOWer solves the URANS/IDDES equations on block-structured grids, and therefore the relative motion of the propeller blades and spinner to the background grid is enabled by the Chimera technique. Body-fitted meshes are generated for these elements, i.e. propeller blades, spinner and nacelle, within a Cartesian background mesh featuring hanging grid nodes, as can be seen in Figure 2. Far-field boundary reflections are mitigated by extending the domain to 100 propeller radii in all directions. The boundary layers of the structural elements are sufficiently resolved to meet the criterion of $y^+ < 1$. Cell extrusion employs a growth rate of 1.15, converging to a cell size of 5 % of the propeller chord length. To establish quasi-stationary conditions and to eliminate transient flow influences, 20 full propeller revolutions are simulated, with the last two revolutions dedicated to acoustic evaluation. The time step is chosen to be $0.5\,^\circ$ for the URANS simulation to adequately capture the acoustic phenomena. For the IDDES simulation, the time step is reduced to $0.25\,^\circ$ based on existing experience with hybrid URANS/LES approaches in FLOWer [23]. Notably, it has been checked that a time step of 0.125° yields no significant impact on the results.

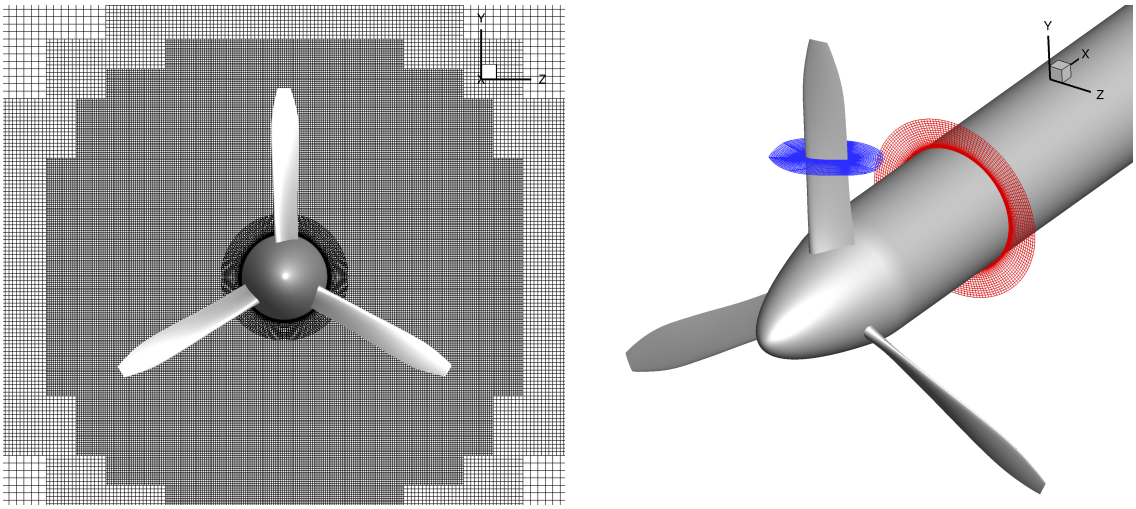

(a) **Background mesh** (b) **Body-fitted meshes**

Fig. 2 CFD mesh.

As mentioned previously, the URANS and IDDES simulations are compared to results obtained with the Lattice-Botzmann method in combination with very large eddy simulations performed with PowerFLOW. For the comparisons made in this paper, results from the LBM simulations with a $y^+ \leq 10$ are considered. A detailed description of the LBM setup can be found in the relevant literature [11]. To assess far-field acoustics, the Ffowcs Williams - Hawkings analogy [25] is utilized by the in-house code ACCO [26]. Notably, in contrast, the results from the LBM simulation are post-processed with SIMULIA PowerACOUSTIC using Farassat's formulation 1A [27]. Nevertheless, for both, the blade surfaces serve as acoustic integration surfaces, capturing noise sources originating directly from the blades. The noise levels are compared at far-field observer positions at a distance of 10 D from the propeller center. Hereby, Θ

represents the fly-over noise directivity and Ψ the azimuthal noise directivity, see Figure 1. Since the noise directivity of an isolated propeller is symmetrical for the azimuthal observer positions, only the fly-over directions are considered for the acoustic evaluation.

For comparison purposes and to directly compare the tonal noise among the several methods, Hanson's model is evaluated using an in-house code of TU Delft [28]. Nevertheless, since the paper focuses in particular on the capability of the several CFD methods, a detailed description of the method is omitted, and reference is made to the relevant literature [7]. For the noise evaluation with Hanson's model, only the first harmonic is investigated, utilizing the load (thrust and torque) distribution of the blade directly. This enables the evaluation of tonal noise arising from the propeller loads without considering broadband noise contributions and the differences that might result from the different FW-H calculations, i.e. ACCO and SIMULIA PowerACOUSTIC. Thus, Hanson's model is used more as a diagnostic tool to better understand and separate the differences between the investigated CFD/CAA workflows.

III. Grid Sensitivity Study

The meshes used in this work for the URANS and IDDES simulations with FLOWer are examined with regard to their influence on the simulation results. Three meshes with different spatial resolutions are therefore created, and URANS simulations are performed with the respective mesh. Since the IDDES simulations require a fine resolution of commonly used $\Delta s/c = 5$ % in FLOWer [23], only URANS simulations are performed for the grid study.

Table 1 Grid parameters.

Resolution	$\Delta s/c$[%]	Growth factor [-]	# Cells blade [$\times 10^6$]	# Cells total [$\times 10^6$]
coarse	15	1.25	1.70	14.3
medium	10	1.20	2.00	25.6
fine	5	1.15	2.35	54.1

The meshes are characterized by their dependence on the propeller chord length commonly used in the literature [29, 30]. In addition, the meshes of the spinner and nacelle are adapted so that they have the same cell size as the propeller blades.

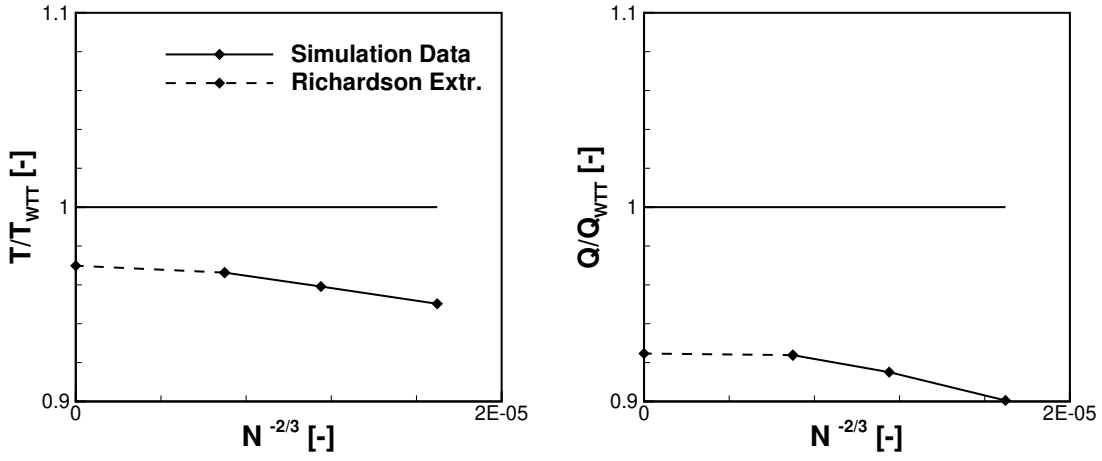

(a) **Thrust** (b) **Torque**

Fig. 3 Grid sensitivity study in positive thrust condition using URANS compared to experimental data [9].

Since the chimera technique is used, the resolution of the background mesh is also adapted to the individual cases, which has a significant effect on the total cell count. Notably, the spatial resolution of the surfaces is not changed to

facilitate the study, which therefore only the volume mesh is affected. The resulting geometric specifications of the associated meshes can be derived from Table 1. From this, the propeller thrust (T) and torque (Q) are evaluated as observation values, and the Richardson extrapolation [31] is performed, which provides the limit solution independent of the grid resolution. For the extrapolation, a method proposed in the literature is applied [32, 33]. The values are then compared without wind tunnel corrections to the experimental data obtained from wind tunnel tests (WTT) conducted at TU Delft [9]. Figure 3 illustrates the convergence of thrust and torque values by refining the mesh. The observed values are plotted against the number of grid cells (N). It is found that by refining the grid, the values converge towards the experimental data, although for each grid (coarse, medium and fine), there is a moderate difference to the experiment of below 5 % for thrust and below 10 % for torque. As can be seen, Richardson's extrapolation provides the least difference to the experiment. This study shows that for the URANS simulation, a resolution of $\Delta s/c = 10\,\%$ may be sufficient to reproduce the aerodynamic physics. However, to maintain a comparison with the same mesh as used for the IDDES simulations, a grid resolution of $\Delta s/c = 5\,\%$ is used for both methods.

IV. Aerodynamic Results

A. Propeller Loading

First, the propeller loads, i.e. thrust and torque, are examined for the two defined operating cases. As can be seen, the integral propeller values of thrust and power are well predicted by FLOWer as compared to experiments, both using URANS and IDDES simulations. Table 2 shows the difference between the respective numerical methods for both advance ratios to the experiments of TU Delft [9].

Table 2 Differences in integral propeller loads to experiments [9].

Solver	Method	J [-]	ΔC_T [%]	ΔC_P [%]	$\Delta \eta_p$ [%]	$\Delta \eta_t$ [%]
FLOWer	URANS	0.6	- 3.0	- 7.7	+ 4.7	-
FLOWer	IDDES	0.6	- 7.9	- 10.3	+ 2.2	-
PowerFLOW	LBM	0.6	- 3.0	- 8.4	+ 5.9	-
FLOWer	URANS	1.1	- 5.3	- 2.3	-	+ 2.9
FLOWer	IDDES	1.1	- 4.5	- 1.6	-	+ 2.8
PowerFLOW	LBM	1.1	-0.8	+ 0.0	-	+ 0.8

The deviations of the URANS simulation are close to the deviations of the LBM simulation at $J = 0.6$, while the differences at $J = 1.1$ are significantly higher for the URANS simulations. Remarkably, the differences in the positive thrust case with the IDDES simulation are higher than with URANS and LBM. Notably, even though an advance ratio of $J = 0.6$ produces positive thrust, it does not correspond to the on-design point, resulting in a more complex flow field at the blade tip. By considering the case of negative thrust, the IDDES simulation shows a smaller error as compared to the URANS simulation when benchmarked against experimental data. Nevertheless, the LBM simulation shows the smallest discrepancies from the experiment in this condition, while all methods are in good overall agreement with the experimental data. Additionally, the distributed loads of thrust and torque are analyzed and compared between the methods, see Figure 4 and Figure 5. Since the integral loads are in a good agreement, the distributed loads are investigated, showing a similar shape. For the thrust distribution in the $J = 0.6$ condition (see Figure 4a), a difference can be found near the tip of the propeller blade. Here, the IDDES simulation shows a decrease of the thrust to negative values, whereas the URANS and LBM simulations are on a similar level. This explains the lower integral thrust in the IDDES simulation. However, the behavior in the tip region, obtained by the IDDES simulation, towards negative values is closer to the measured results from the experiments, which will be demonstrated by the evaluation of the total pressure in the propeller slipstream. In the negative thrust regime, see Figure 4b, there are no significant differences between the methods. All methods predict a similar shape of the thrust distribution, with values in a comparable range.

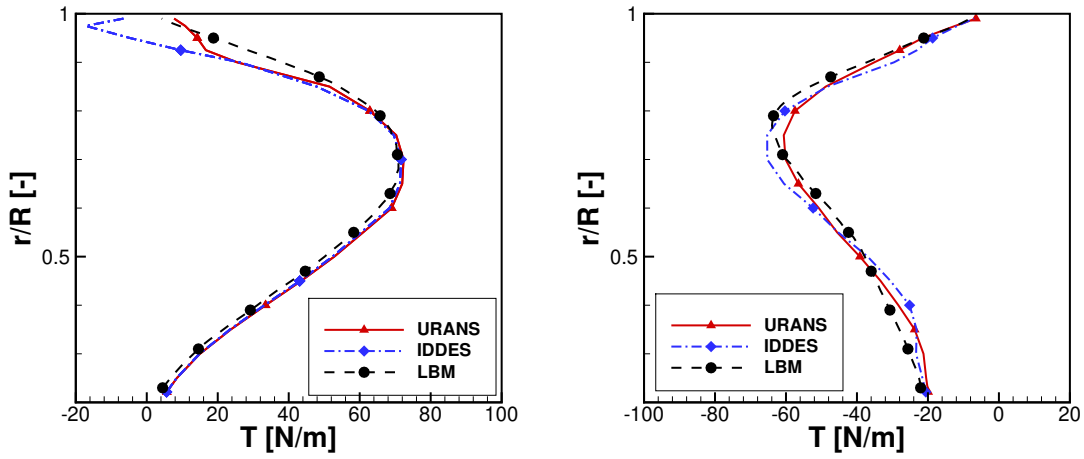

(a) **Positive thrust condition: J = 0.6** (b) **Negative thrust condition: J = 1.1**

Fig. 4 Distributed thrust on blade.

This confirms the good agreement of the integral thrust for this particular operating point. Observing the propeller torque in the positive thrust case (Figure 5a), it can be seen that the URANS simulation exhibits a kink at $r/R = 0.85$, which is not the case for the IDDES and LBM simulations. In the negative thrust regime (see Figure 5b), the shape of the torque distribution is also comparable for all methods, while the magnitude is lower in the middle blade section for the LBM simulation.

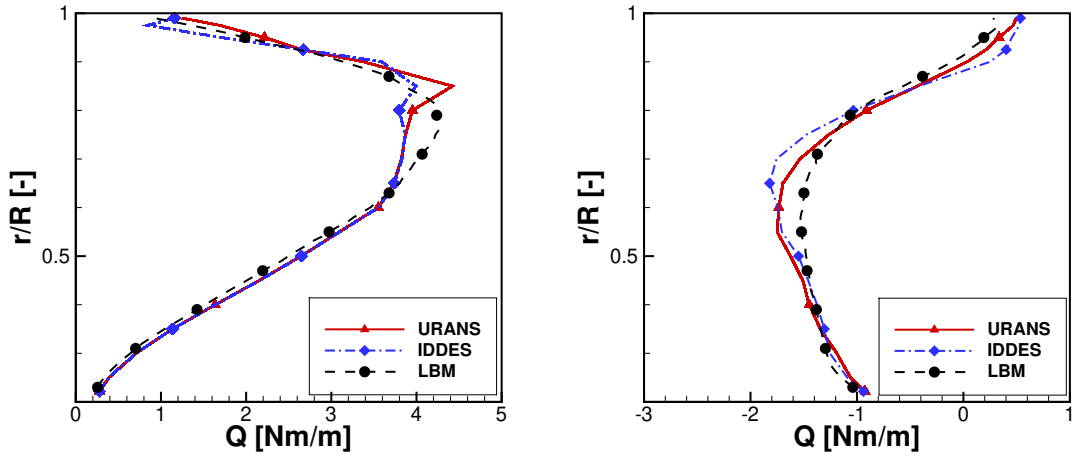

(a) **Positive thrust condition: J = 0.6** (b) **Negative thrust condition: J = 1.1**

Fig. 5 Distributed torque on blade.

This comparison serves as the basis for the acoustic evaluation, since thrust and torque contribute to the noise emission of the propeller. It also shows that all methods are capable of predicting loads with differences being below 8 % in thrust and 11 % in torque in the positive thrust case and respectively below 6 % in thrust and below 3 % in torque for the negative thrust case.

B. Total Pressure in the Wake

Since the distributed loads of the propeller can only be compared between the numerical methods, the investigation of the total pressure in the propeller slipstream enables a further comparison to the experiments [34]. Furthermore, this study helps to understand the capability of reproducing the flow physics of the respective numerical method. As mentioned in the previous section, the total pressure in the slipstream of the propeller is determined in a plane perpendicular to the plane of propeller rotation, i.e. $x/R = 0.15$, as shown in Figure 6.

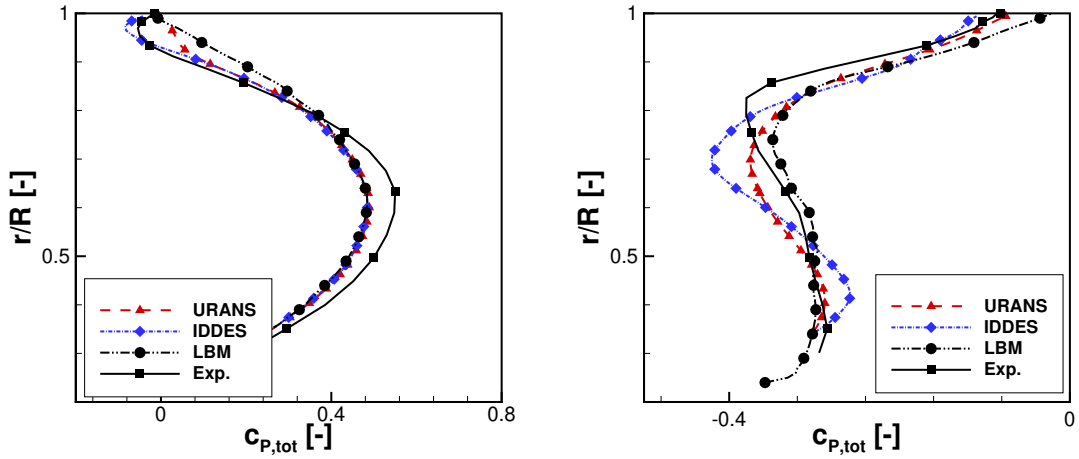

(a) **Positive thrust condition: J = 0.6**

(b) **Negative thrust condition: J = 1.1**

Fig. 6 Total pressure in the wake of propeller compared to experiments [9].

Here, the previously mentioned statement (see subsection IV.A) in the positive thrust regime of the effect at the blade tip, where the IDDES simulation predicts negative thrust values, becomes evident. While the URANS and LBM simulations show a similar characteristic in the tip region, the IDDES simulation and the experiment show a negative total pressure here. Overall, all methods are in good agreement with the experiment in the positive thrust regime regarding the shape and magnitude of the total pressure, while the negative thrust regime shows significant differences between the numerical methods. Here, the LBM simulation shows the closest agreement with the experiments, while the IDDES simulation shows significant differences in shape and magnitude, especially in the middle section of the propeller blade, where a lower total pressure is predicted.

C. Surface Pressure

To conclude the aerodynamic study and delve deeper into the different flow phenomena on the propeller blades, which directly affect the noise signature of the propeller, especially at higher harmonics, the surface pressure on the propeller blade is examined and compared for the respective numerical method. Considering that the acoustic results are dominated by the contributions from the outboard part of the blade, where the Mach number is highest, the pressure distributions are examined at $r/R = 70\%$ and $r/R = 90\%$. The results for the positive thrust case are shown in Figure 7. Considering the radial section at $r/R = 70\%$, all methods show a similar trend of the surface pressure over the chord length, with no significant differences in magnitude. However, the LBM simulation shows less negative pressure at the leading edge on the back side of the propeller blade (i.e. in a positive thrust case similar to the pressure side), while the URANS and IDDES simulations predict the same magnitude. Additionally, a slight discrepancy in the shape of the surface pressure curve is found on the back of the blade, while no differences are found on the front side of the blade (i.e. coinciding with the suction side in the positive thrust case). Moving closer to the tip region, greater differences in shape and magnitude are observed for all methods. While again, there are no differences on the front side of the blade, higher discrepancies can be seen in the region of $0 < x/c < 0.5$ on the back side, see Figure 7b. The LBM simulation predicts a less negative surface pressure with a faster decrease after the leading edge. Furthermore, the IDDES simulation predicts a comparable magnitude of surface pressure but shows a higher gradient after the leading edge, with a good agreement between the methods in the region of the trailing edge. It is assumed that the different size

of the separation bubble is responsible for the discrepancies here. With this, the differences in thrust towards the tip region can be explained. Nevertheless, overall, the methods show a similar trend in surface pressure, except on the back side near the leading edge. This explains the differences in the integral loads discussed in subsection IV.A, but also shows that despite the differences in the surface pressure, the integral loads are in a good agreement.

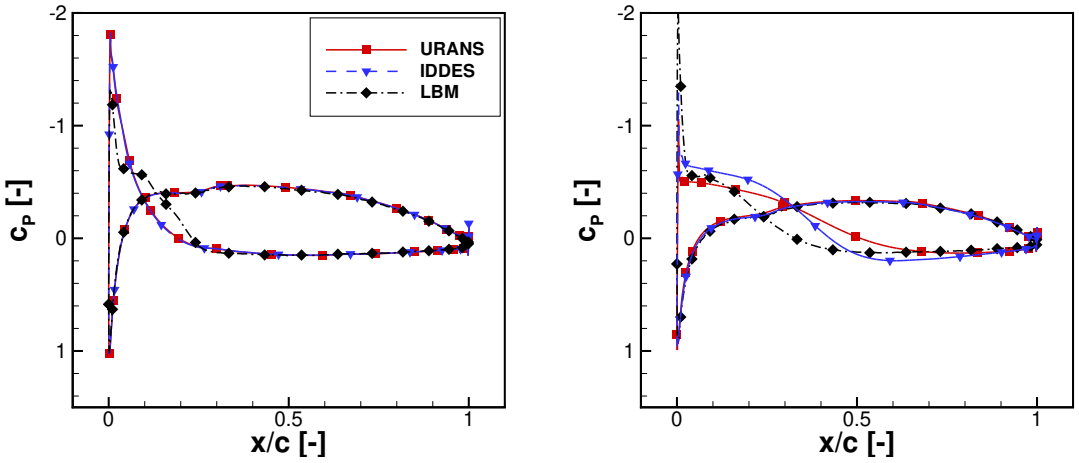

(a) **r/R = 70 %** (b) **r/R = 90 %**

Fig. 7 Surface pressure on propeller blade - J = 0.6.

Considering the negative thrust regime, both radial positions on the propeller are analyzed accordingly as illustrated in Figure 8, where for both sections no differences are found on the front side of the blade (i.e. the pressure side in the negative thrust case). Conversely, on the back side of the blade at $r/R = 70\%$ (i.e. suction side in the negative thrust regime), larger differences occur due to a separation bubble, which is described in the literature [8]. While the result from the URANS simulation follows the trend of the LBM simulation, the IDDES simulation predicts an increase in suction pressure in the range of $0.4 < x/c < 0.7$, see Figure 8a.

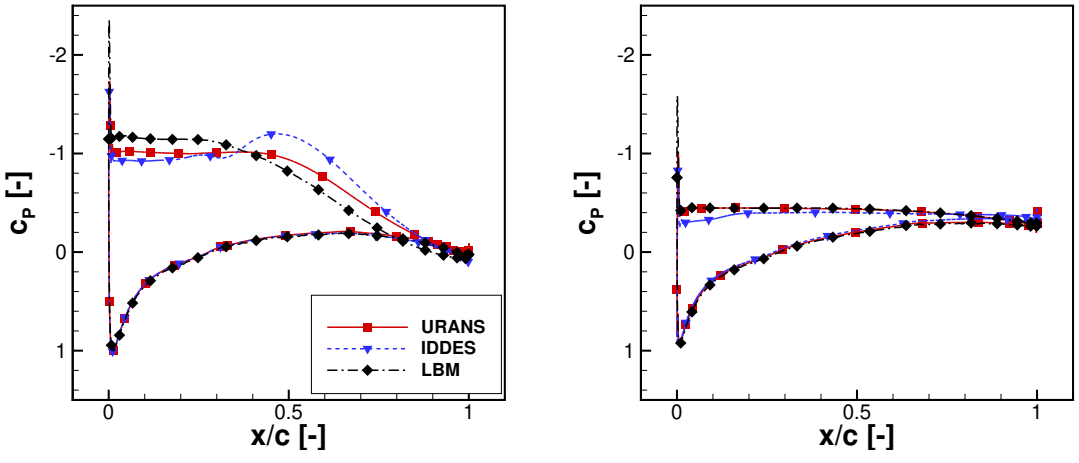

(a) **r/R = 70 %** (b) **r/R = 90 %**

Fig. 8 Surface pressure on propeller blade - J = 1.1.

Nevertheless, all methods show a similar trend with respect to the studied separation on the back side of the blade [8]. In the tip region of the propeller blade, no significant differences are observed between the methods, see Figure 8b. This

is in agreement with the investigations made by observing the total pressure in the wake, where the highest differences occur in the region of $r/R = 70\%$.

V. Sound Pressure Time Signature and Spectral Analysis

First, the time-resolved sound pressure obtained from the different numerical methods is evaluated at a specific observer location in the propeller plane ($\Theta = 90\,^{\circ}$). Therefore, two revolutions from the CFD simulation are used as input for the FW-H calculation. The time signatures for the both cases are shown in Figure 9 over one full revolution. All methods predict a clear sinusoidal contour emitted at the blade passing frequency (BPF) in the positive thrust case. In contrast to the URANS and IDDES simulations, the LBM simulation also shows higher-frequency contributions from broadband noise. Looking at the negative thrust case, it can be seen that the URANS simulation still shows a sinusoidal signal emitted at the BPF, but with a significantly reduced amplitude compared to the positive thrust case. However, the IDDES and LBM simulations show large contributions of broadband fluctuations, where the underlying BPF tone is no more visible for the LBM simulation and the broadband fluctuations are significantly higher compared to the IDDES simulation results.

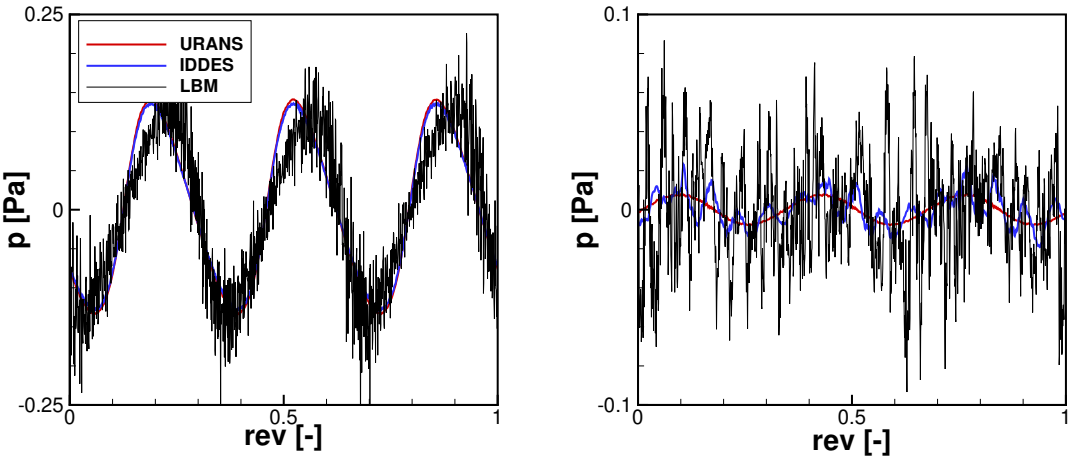

(a) **Positive thrust condition: J = 0.6**

(b) **Negative thrust condition: J = 1.1**

Fig. 9 Time-resolved sound pressure at $\Theta = 90°$.

To see the spectral contributions, an FFT analysis is performed. The periodized signal of two revolutions is used for the analysis for the respective method. Furthermore, the results of all methods are post-processed in the same manner, which enables a direct comparison in terms of frequency resolution. Figure 10a shows that the first three harmonics are in a good agreement for all methods in the positive thrust case, while the first BPF clearly dominates the spectrum. As expected from the time signal, broadband noise is present at higher frequencies for the LBM simulation, where URANS and IDDES predict significantly lower amplitudes. For the negative thrust case, broadband noise is more pronounced for the IDDES and LBM simulations, as is expected, since LBM and IDDES simulations are capable of resolving parts of the smaller turbulent structures in contrast to the URANS simulation, see Figure 10b. However, the URANS simulation shows a similar amplitude at the first BPF harmonic compared to the IDDES simulation and LBM simulation. While the first BPF amplitude is similar between all methods, the usage of the IDDES simulation enables to capture parts of the broadband noise fluctuations, which results in a significant amplification of noise levels at higher frequencies compared to the URANS simulation. Nonetheless, the amplitude of noise levels seems to be still lower than predicted by the LBM simulation. Furthermore, the URANS simulation predicts no increase in broadband noise compared to the positive thrust case due to the limited representation of the broadband fluctuations. Finally, this shows that the URANS simulation is still capable of predicting similar tonal noise characteristics at the first BPF compared to the IDDES and LBM simulations but fails to capture the amplitude at higher frequencies in the negative thrust case. Furthermore, it shows that the URANS simulation is a good choice for obtaining accurate predictions of the higher harmonics in several directions in the positive thrust case, which will be further demonstrated by analyzing the overall noise directivity.

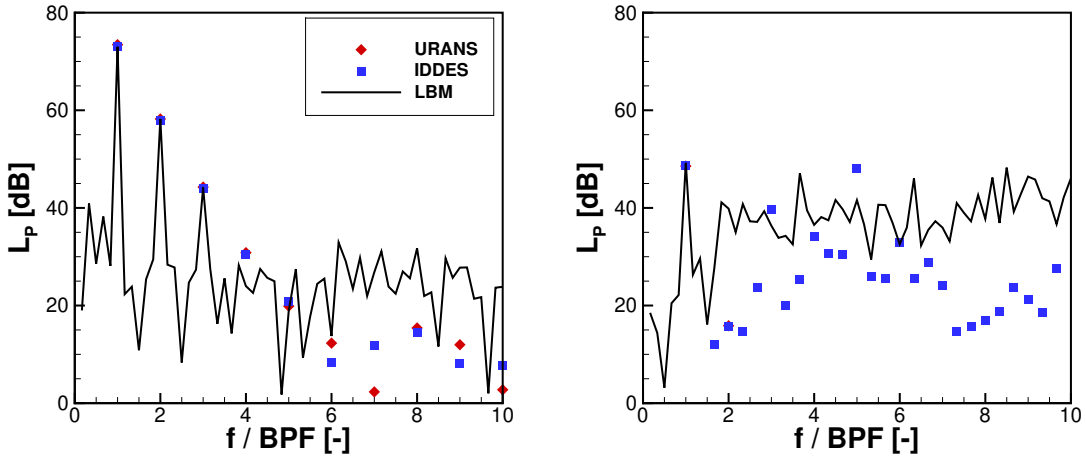

(a) **Positive thrust condition: J = 0.6** (b) **Negative thrust condition: J = 1.1**

Fig. 10 FFT analysis at $\Theta = 90°$.

VI. Noise Evaluation

A. Thickness and Loading Noise Contributions - 1.BPF

To study the noise directivity, several observer positions perpendicular to the propeller plane are investigated, defined as Θ-directivity. Since all methods use the FW-H formulation to propagate the noise to the far-field observers, a separation of the several noise source contributions is performed. The integration surface for the FW-H formulation coincides with the physical surfaces of the propeller blades, thus ignoring the quadrupole contribution. Notably, the LBM simulation solves the FW-H equation by the Farassat 1-A formulation, while for the URANS and IDDES methods the FW-H equation is solved by the in-house code ACCO, which also allows the source-time consideration of mean flow effects [35]. However, both methods provide information about the contribution of the thickness (monopole) and loading (dipole) noise sources for the first BPF, which are shown in Figure 11 and Figure 12 for the positive and negative thrust setting, respectively.

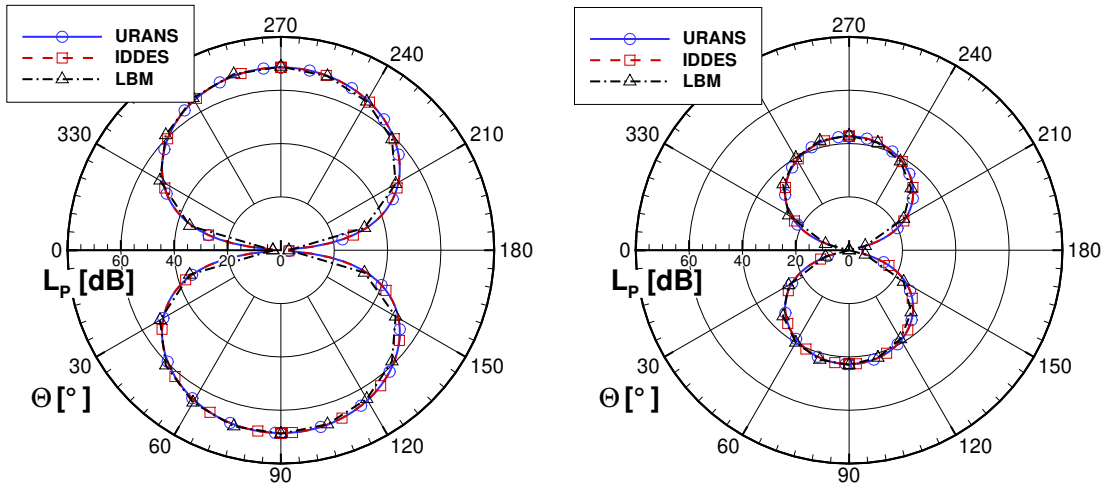

(a) **Positive thrust condition: J = 0.6** (b) **Negative thrust condition: J = 1.1**

Fig. 11 Noise directivity of the monopole source contribution - 1.BPF.

It can be seen that in both thrust cases, the thickness noise has a similar noise directivity in shape and magnitude for all methods. This is as expected because the monopole noise source is related to the geometric definition of the propeller blade, which is similar for all methods. It is noteworthy that, when comparing the two advance ratios, the emitted noise is significantly reduced when considering the negative thrust case, which corresponds to the reduced Mach number due to the lower rotational speed of the propeller, see Figure 11.

Conversely, by observing the loading noise contribution, there are discrepancies between the methods in the negative thrust case, while for the positive regime, all methods predict a similar magnitude of noise at the first BPF, see Figure 12. Interestingly, both contributions, thickness and loading, have a comparable magnitude in the noise directivity in the positive thrust regime. This does not seem to be the case in the negative thrust regime, where the loading noise is higher than the thickness noise. Furthermore, as already shown in section V, all methods show the same magnitude in the directions $\Theta = 90\,^\circ$ and $\Theta = 270\,^\circ$. In contrast, in the flow directions, i.e. $\Theta = 0\,^\circ$ and $\Theta = 180\,^\circ$, the noise is higher for the IDDES and LBM simulations than for the URANS simulation. Although only the BPF is considered in this study, it is assumed that broadband noise contributions are superimposed on the tonal noise, leading to the noise increase in these directions also at this frequency. In addition, since the URANS simulation shows no noise emission in these directions, it can be assumed that the broadband noise is dominant in these directions. Here, the IDDES and LBM simulations exhibit a similar characteristic and amplitude of noise levels.

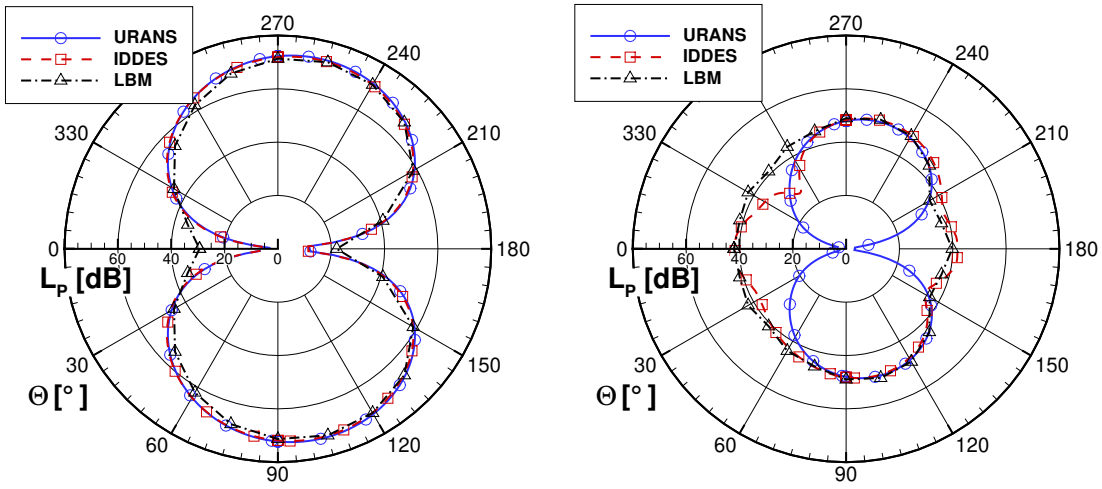

(a) **Positive thrust condition: J = 0.6**

(b) **Negative thrust condition: J = 1.1**

Fig. 12 Noise directivity of the dipole source contribution - 1.BPF.

B. Overall Noise

Additionally, the overall noise level and the sum of both noise source contributions, referred to as total noise, for the first BPF are evaluated in Figure 13 and Figure 14. If only the first BPF is considered (total noise), all methods show a similar shape and amplitude of the noise directivity in the positive thrust regime, which is consistent with the previous shown results, see Figure 13a. In the negative thrust regime, the total noise agrees well when comparing the IDDES and LBM simulation results, where higher noise levels are emitted in streamwise directions as already observed for the loading noise contribution, which is illustrated in Figure 13b. This shows that broadband noise is dominant in these directions, where the URANS simulation shows lower results due to the missing broadband contributions. Overall the comparison is similar to the investigations made for the loading noise contribution, showing the major impact of loading noise on the total noise compared to thickness noise for these operation cases. Considering the overall sound pressure level, i.e. the sum of all frequencies, it can be seen that the results from the URANS and IDDES simulations are comparable in magnitude and shape to the total noise directivity in the positive thrust case, see Figure 14a. In contrast, the results from the LBM simulation agree well in the directions $\Theta = 90\,^\circ$ and $\Theta = 270\,^\circ$, but differ in the streamwise direction. This can be explained by the contribution of broadband noise, where the LBM simulation shows

high contributions, and IDDES or URANS simulations show no broadband noise in these specific directions.

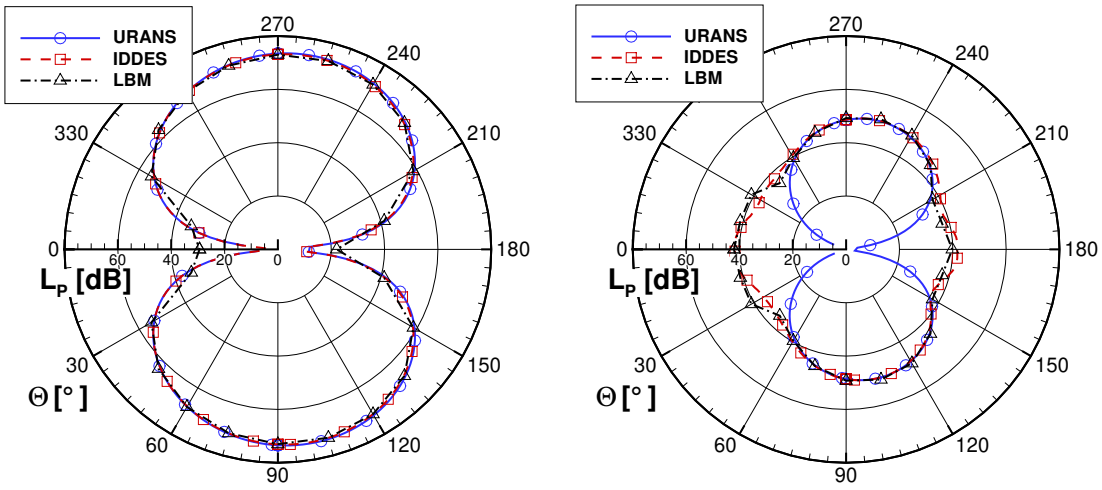

(a) **Positive thrust condition: J = 0.6** (b) **Negative thrust condition: J = 1.1**

Fig. 13 Total noise directivity - sum of monopole and dipole contributions.

In the negative thrust case, the highest noise is emitted in the streamwise direction (i.e. $\Theta = 0\,^\circ$ and $\Theta = 180\,^\circ$) for the LBM and IDDES simulations, while the URANS simulation shows only a slight increase in overall noise in these directions, see Figure 14b. The IDDES and LBM simulations agree well on the shape but still differ in magnitude, about 5 dB, of the overall noise directivity, which can be explained by the dominant broadband noise, which is differently predicted by both simulations. Notably, the slight increase in streamwise direction from the URANS simulation indicates that there is still a small contribution of broadband noise captured.

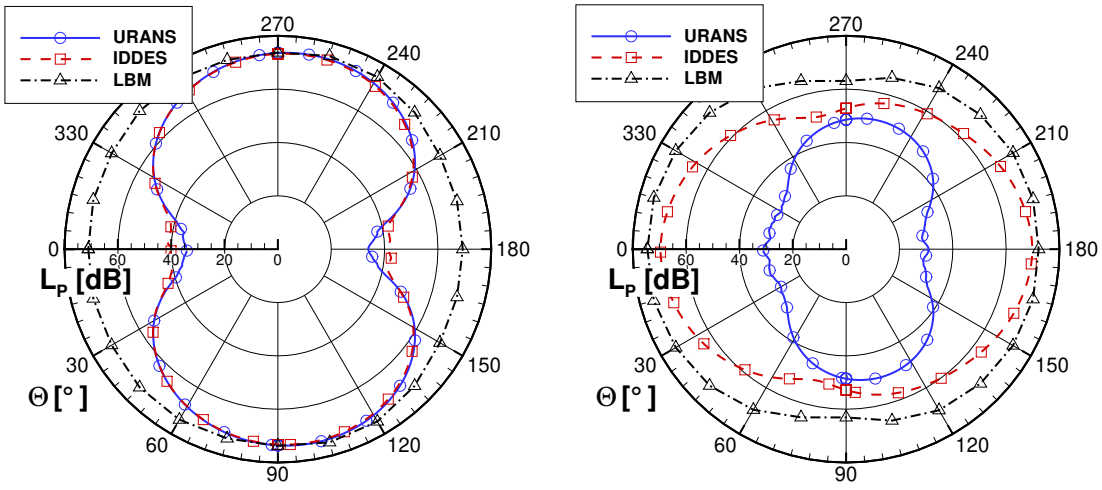

(a) **Positive thrust condition: J = 0.6** (b) **Negative thrust condition: J = 1.1**

Fig. 14 Overall noise directivity.

C. Hanson's Model

Finally, a low fidelity acoustic evaluation by Hanson's model is performed using the CFD results from all methods. For this purpose, the solver implemented at TU Delft is used [28]. Subsequently, the shown load distributions are used

as input to the solver, and the noise directivity at the defined observer positions is determined for the first BPF. First, a comparison is made between the results of Hanson's model and the FW-H formulation using the URANS simulation data as input Figure 15. This will conclude the computational cross-validation study by showing further possibilities and limitations of different simulation fidelity, since in the literature several combinations of CFD/CAA methods are commonly used. Furthermore, the application of Hanson's model can save computational time by performing for these cases $< 1\,\text{sec}$, while the acoustic evaluation with ACCO took about 85 sec on 4096 cores, resulting in about $100\,\text{core} - \text{h}$. As can be seen for both thrust cases, a good agreement is achieved by Hanson's model when compared to the results from the FW-H formulation.

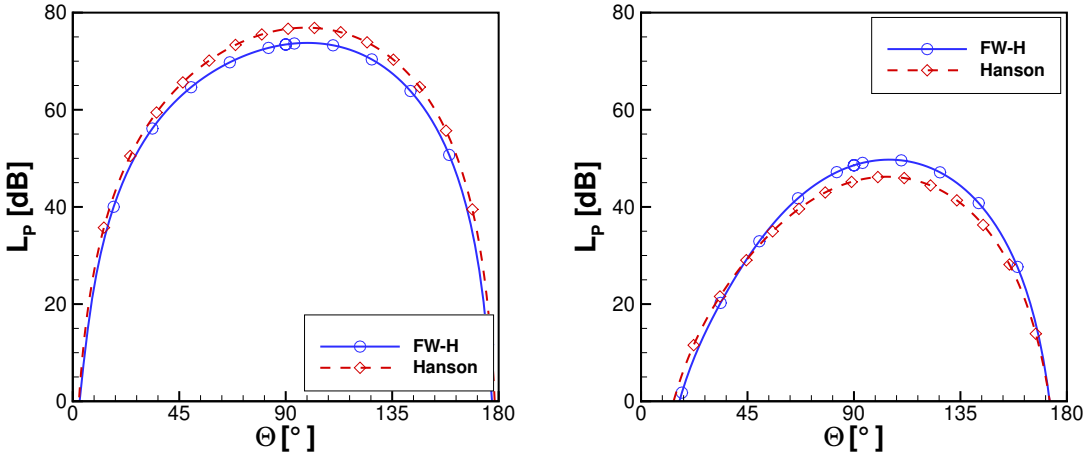

(a) **Positive thrust condition: J = 0.6** (b) **Negative thrust condition: J = 1.1**

Fig. 15 Comparison of Hanson's model results and FW-H results using URANS simulation data.

Nevertheless, an overprediction of about 3 dB of the maximum noise level in the direction $\Theta = 90\,°$ can be found for the positive thrust case, see Figure 15a. Conversely, in the negative thrust case, Hanson's model predicts the maximum noise level about 3 dB lower than the FW-H formulation, as illustrated in Figure 15b.

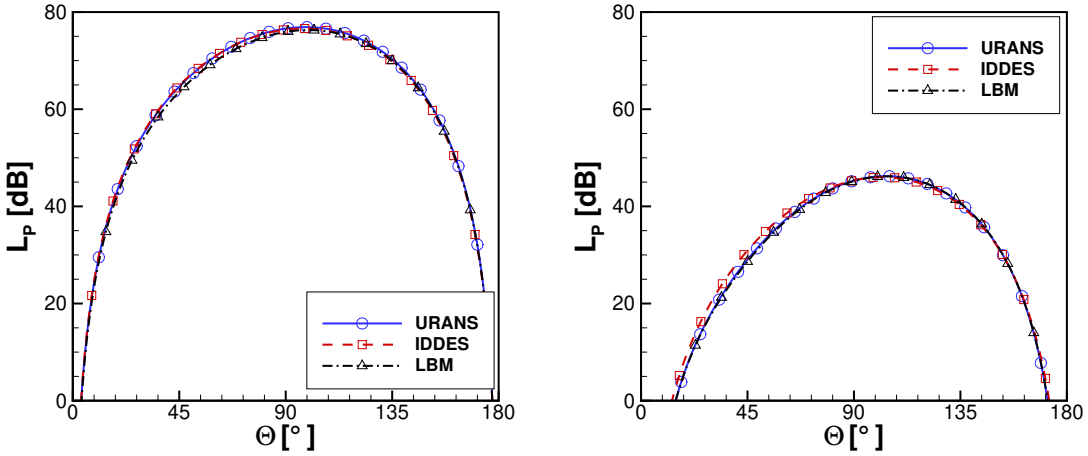

(a) **Positive thrust condition: J = 0.6** (b) **Negative thrust condition: J = 1.1**

Fig. 16 Comparison of Hanson's model results using different CFD simulation data.

Furthermore, in both thrust cases, the shape of the noise directivity is in a good agreement compared to the

application of the FW-H formulation. Thus, Hanson's model is well suited to predict the tonal noise directivity for both thrust cases, but the differences in magnitude have to be taken into account, which might result from simplifications made in Hanson's model. As expected, since the load distributions for thrust and torque are in good agreement for both advance ratios, the noise directivity is also in a good agreement for all methods, which can be seen in Figure 16. Nonetheless, it shows that the increase in tonal noise in streamwise directions, which was shown for the IDDES and LBM simulations in subsection VI.A and subsection VI.B is obviously not captured by Hanson's model. Thus, the combination of higher-fidelity methods like LBM and IDDES simulations in combination with Hanson's model reduces the quality of the noise prediction significantly, while the combination with URANS simulations seems to be feasible in both operation conditions.

D. Influence of Blending Function

Given the partly non-periodic nature of the flow field, particularly evident in the negative thrust case, a blending function can be employed for acoustic evaluation in ACCO, enforcing the periodicity of pressure waves [35]. This enables the consideration of numerous revolutions, which are needed especially for fly-over noise simulation, by only using the CFD data of one or two revolutions, reducing significantly the computational time. Therefore, this study investigates the influence of the blending width on the noise directivity. While for all shown results no blending was used, the effect of using a blending function will be discussed here. As shown, the IDDES simulation for the negative thrust case generates higher contributions of broadband noise, therefore the results from the IDDES simulations are used for this study. Contrarily, the URANS simulation provides a mostly perfect sinusoidal signal, where the blending function did not affect the noise signature. Here, three blending widths are investigated to evaluate the relative differences between the approaches. In addition, an evaluation without periodicity and therefore without a blending function (similar to the previously presented results from the IDDES simulations) is used as a reference to show the influence on the noise directivity. As can be seen in Figure 17a, the blending width affects the tonal noise directivity in the negative thrust case mainly in the directions where broadband noise is dominant. There are no differences in the directions $\Theta = 90\,^\circ$ and $\Theta = 270\,^\circ$. Conversely, the noise level is reduced by 10 dB in the directions $\Theta = 0\,^\circ$ and $\Theta = 180\,^\circ$ by using a longer blending width. This explains why a longer blending width eliminates more broadband noise, while the shortest blending width of a blade passage, i.e. 1/3 revolution, best matches the unblended result. Furthermore, it can be seen that the noise directivity is affected in its symmetry. Finally, the overall noise levels in the negative thrust regime are compared for the different blending widths. No difference is found in the shape of the noise directivity and there is also no significant influence on the magnitude. Thus, the blending function diminishes some parts of the broadband contributions but is still able to predict a similar noise directivity in the case where broadband noise is dominant. Finally, it can be said that it is recommended to use the shortest possible blending width if considering fly-over noise simulations with IDDES simulation results.

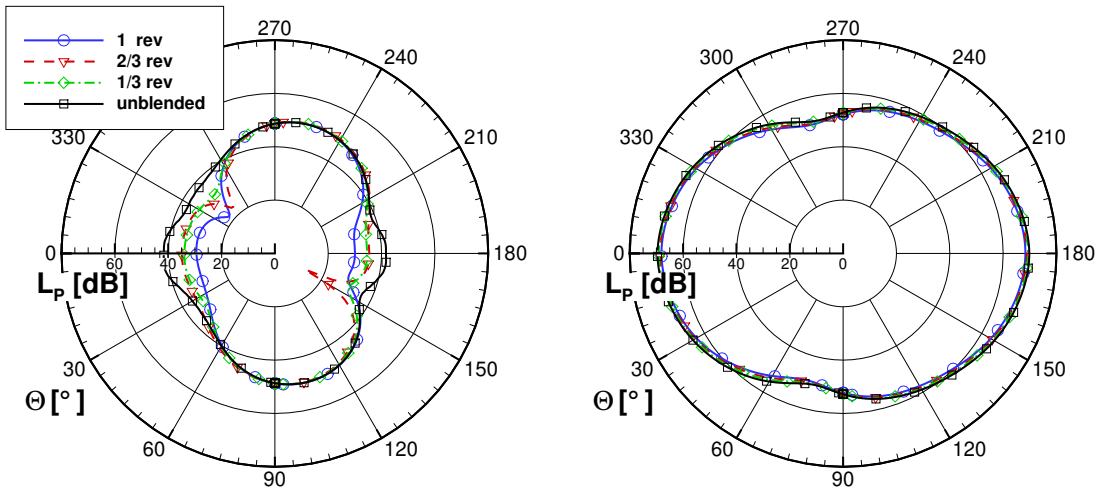

(a) **Tonal noise (1.BPF)** (b) **Overall noise**

Fig. 17 Influence of blending width.

VII. Conclusions

This study applied different levels of fidelity in CFD and CAA simulations to an isolated propeller operating in positive and negative thrust conditions. Different methods from URANS, IDDES to LBM VLES are considered and compared with experimental results from the literature regarding aerodynamic behavior. It was shown that the propeller loads are in good agreement between the numerical methods and differ below 8 % in thrust and 11 % in torque from the experimental results obtained in the wind tunnel of TU Delft. Furthermore, the flow field characteristics were analyzed to study the effect of the scale-resolving IDDES simulation, and it was found that significant differences between the methods occurred due to the different predictions of separation. To compare the experimental results with the simulation methods, the total pressure in the propeller slipstream was compared, where it was shown that all methods predict the same trend in the positive regime, while the IDDES simulation showed significant differences in the negative thrust regime. This was supported by an analysis of the propeller surface pressure at two exemplary radial slices. As expected, in the positive regime, the comparison between the methods is comparably good, but a different trend of the surface pressure was found at a radial position $r/R = 70\%$. For the negative thrust case, the IDDES simulation predicted an increase in surface pressure after a separation bubble on the back side of the blade, which was not found for the URANS and LBM simulations. This explained the differences in the total pressure, which occurred mainly in the middle section behind the propeller blade.

The aerodynamic study was performed as the basis for the acoustic analysis. With that, the time signature and FFT analysis revealed that the tonal noise dominates in the positive thrust case, when using URANS and IDDES simulations, while the broadband noise increased significantly in the negative thrust regime. This effect was not captured by the URANS simulation, while in the positive thrust case, all methods showed a similar characteristic and magnitude of noise levels, justifying the application of URANS simulations for propulsive conditions without significant separations on the propeller blade. This study also showed the differences by using the URANS simulation for separated flows and the effect on the acoustics. It was shown that the URANS simulation is still able to predict the tonal noise accurately compared to the IDDES and LBM simulations under these conditions in several directions but failed to predict the noise levels in the streamwise directions, where broadband noise was dominant and superimposed with the tonal noise. Obviously, the overall noise was different due to the omitted broadband noise when using the URANS simulation data, mainly in the directions where broadband noise dominates the tonal noise, i.e. in the streamwise directions. By employing IDDES simulations, tonal noise was found to be in a good agreement with the LBM simulation results due to the partly captured broadband fluctuations. Nevertheless, for the overall noise, the IDDES simulation predicted lower values, about 5 dB compared to the LBM simulation results. Lastly, a comparison to the results of Hanson's model revealed the limitations of the simplified approach, particularly for tonal noise superimposed by broadband noise, which is not captured by the method.

Finally, insights into the quality of aeroacoustic predictions are given, which can be further used for trade-offs between accuracy and computational effort. Here, it was found that through using the URANS simulation compared to the IDDES simulation in FLOWer the computation time was reduced about 40 % using the same mesh but different time step. This is of particular interest when considering distributed propulsion with a single recuperating propeller. Here, as shown, computationally intensive scale-resolving methods would not be needed for the propulsive DEP propellers, while the recuperating propeller would lack broadband noise information. Nevertheless, tonal noise predictions could be performed in several directions without broadband noise, still capturing the accurate noise levels in some directions.

Acknowledgments

The authors gratefully acknowledge the Federal Ministry for Economic Affairs and Climate Action (BMWK) for funding this work in the framework of the research project eMission (FKZ: 20M2248). Further thanks to the High Performance Computing Center (HLRS) in Stuttgart for providing the computational resources, as well as support and service for the use of the Hawk cluster.

Supported by:

on the basis of a decision
by the German Bundestag

References

[1] Kim, H. D., Perry, A. T., and Ansell, P. J., "A Review of Distributed Electric Propulsion Concepts for Air Vehicle Technology," *AIAA/IEEE Electric Technologies Symposium*, 2018. https://doi.org/10.2514/6.2018-4998.

[2] Firnhaber-Beckers, M., Schollenberger, M., Lutz, T., Bongen, D., Radespiel, R., Florenciano, J. L., and Funes-Sebastian, D. E., "CFD Investigation of High-Lift Propeller Positions for a Distributed Propulsion System," *AIAA Aviation, Chicago*, 2022. https://doi.org/10.2514/6.2022-3217.

[3] Deere, K., Viken, S., Carter, M., Viken, J., Wiese, M., and Farr, N., "Computational Analysis of Powered Lift Augmentation for the LEAPTech Distributed Electric Propulsion Wing," *AIAA Aviation Denver*, 2017. https://doi.org/10.2514/6.2017-3921.

[4] Firnhaber Beckers, M., Schollenberger, M., Lutz, T., Bongen, D., Radespiel, R., Florenciano, J. L., and Funes-Sebastian, D. E., "Numerical Investigation of High-Lift Propeller Positions for a Distributed Propulsion System," *Journal of Aircraft*, 2023. https://doi.org/10.2514/1.C037248.

[5] Schollenberger, M., Kirsch, B., Lutz, T., Krämer, E., and Friedrichs, J., "Aerodynamic interactions between distributed propellers and the wing of an electric commuter aircraft at cruise conditions," *CEAS Aeronautical Journal*, 2024. https://doi.org/10.1007/s13272-023-00706-6.

[6] Hedrick, W. S., and Douglass, W. M., "An Experimental Investigation of the Thrust and Torque Produced by Propellers Used as Aerodynamic Brakes," *Tech. Rep. NACA- WR-A-27, National Advisory Committee for Aeronautics*, 1944. https://doi.org/http://hdl.handle.net/2060/19930093338.

[7] Goyal, J., Avallone, F., and Sinnige, T., "Isolated propeller aeroacoustics at positive and negative thrust," *Aerospace Science and Technology*, Vol. 147, 2024. https://doi.org/10.1016/j.ast.2024.109021.

[8] Goyal, J., Sinnige, T., Ferreira, C., and Avallone, F., "Aerodynamics and Far-field Noise Emissions of a Propeller in Positive and Negative Thrust Regimes at Non-zero Angles of Attack," *AIAA Aviation Forum*, 2023. https://doi.org/10.2514/6.2023-3217.

[9] Nederlof, R., Ragni, D., and Sinnige, T., "Experimental Investigation of the Aerodynamic Performance of a Propeller at Positive and Negative Thrust and Power," *AIAA Aviation Forum*, 2022. https://doi.org/10.2514/6.2022-3893.

[10] Goyal, J., Sinnige, T., Ferreira, C., and Avallone, F., "Aerodynamic and Aeroacoustic Characteristics of an Isolated Propeller at Positive and Negative Thrust," *AIAA Aviation Forum*, 2021. https://doi.org/10.2514/6.2021-2187.

[11] Goyal, J., Sinnige, T., Avallone, F., and Ferreira, C., "Benchmarking of Aerodynamic Models for Isolated Propellers Operating at Positive and Negative Thrust," *AIAA Journal*, Vol. 62, 2024. https://doi.org/10.2514/1.J064093.

[12] Delft University of Technology, "CAD file of the TUD-XPROP," 2024. https://doi.org/10.5281/zenodo.13645390.

[13] Shur, M. L., Spalart, P. R., Strelets, M. K., and Travin, A. K., "A hybrid RANS-LES approach with delayed-DES and wall-modelled LES capabilities," *International Journal of Heat and Fluid Flow*, Vol. 29, 2008. https://doi.org/10.1016/j.ijheatfluidflow.2008.07.001.

[14] Raddatz, J., and Fassbender, J., "Block structured Navier-Stokes solver FLOWer," *Notes on Numerical Fluid Mechanics and Multidisciplinary Design (NNFM)*, Vol. 89, 2005, pp. 27–44. https://doi.org/10.1007/3-540-32382-1_2.

[15] Kowarsch, U., Oehrle, C., Hollands, M., Keßler, M., and Krämer, E., "Computation of Helicopter Phenomena Using a Higher Order Method," *High Performance Computing in Science and Engineering*, 2013, pp. 423–438. https://doi.org/10.1007/978-3-319-02165-2_29.

[16] Schuff, M., Kranzinger, P., Keßler, M., and Krämer, E., "Advanced CFD-CSD coupling: Generalized, high performant, radial basis function based volume mesh deformation algorithm for structured, unstructured, and overlapping meshes," *40th European Rotorcraft Forum, Southampton, UK*, 2014.

[17] Wickersheim, R., Keßler, M., and Krämer, E., "Aeroacoustics of High Fidelity URANS Simulations of Distributed Electric Propellers," *New Results in Numerical and Experimental Fluid Mechanics XIV. STAB/ DGLR Symposium 2022. Notes on Numerical Fluid Mechanics and Multidisciplinary Design, edited byA. Dillmann, G. Heller, E. Krämer, C. Wagner, and J. Weiss*, Vol. 145, 2023. https://doi.org/10.1007/978-3-031-40482-5_33.

[18] Wickersheim, R., Keßler, M., and Krämer, E., "Noise Prediction of a Distributed Propulsion System Using the Actuator Line Method," *AIAA Journal*, 2024. https://doi.org/10.2514/1.J063457.

[19] Kostek, A. A., Lößle, F., Wickersheim, R., Keßler, M., Boisard, R., G., R., Visingardi, A., Barbarino, M., and Gardner, A. D., "Experimental investigation of UAV rotor aeroacoustics and aerodynamics with computational cross-validation," *CEAS Aeronautical Journal*, 2023. https://doi.org/10.1007/s13272-023-00680-z.

[20] Wickersheim, R., Keßler, M., Sembowski, J., Bongen, D., and Gomes, J. P., "Numerical Investigation and Validation of Noise Sources of a Distributed Propulsion System," *AIAA Journal*, 2024. https://doi.org/10.2514/1.J064531.

[21] Borges, R., Carmona, M., Costa, B., and Don, W., "An improved weighted essentially non-oscillatory scheme for hyperbolic conservation laws," *Journal of Computational Physics*, 2008, pp. 3191–3211. https://doi.org/10.1016/j.jcp.2007.11.038.

[22] Menter, F. R., Kuntz, M., , and Langtry, R., "Ten Years of Industrial Experience with the SST Turbulence Model," *Turbulence, Heat and Mass Transfer*, Vol. 4, 2003.

[23] Letzgus, J., Gardner, A., Schwermer, T., Keßler, M., and Krämer, E., "Numerical Investigations of Dynamic Stall on a Rotor with Cyclic Pitch Control," *Journal of the American Helicopter Society*, Vol. 64, 2019. https://doi.org/10.4050/JAHS.64.012007.

[24] Weihing, P., Letzgus, J., Lutz, T., and Krämer, E., "Development of alternative shielding functions for Detached-Eddy Simulations," *Progress in Hybrid RANS- LES Modelling*, 2020. https://doi.org/10.1007/978-3-030-27607-2_8.

[25] Ffowcs Williams, J. E., and Hawkings, D. L., "Sound Generated by Turbulence and Surfaces in Arbitrary Motion," *Philosophical Transactions of the Royal Society of London, Series A: Mathematical and Physical Science*, 1969. https://doi.org/10.1098/rsta.1969.0031.

[26] Keßler, M., and Wagner, S., "Source Time Dominant Aeroacoustics," *Computers & Fluids*, Vol. 33, No. 5-6, 2004, pp. 791–800. https://doi.org/10.1016/j.compfluid.2003.06.012.

[27] Farassat, F., and Succi, G. P., "A review of propeller discrete frequency noise prediction technology with emphasis on two current methods for time domain calculations," *Journal of Sound and Vibration*, 1980. https://doi.org/https://doi.org/10.1016/0022-460X(80)90422-8.

[28] Goyal, J., "Hanson's Model in Frequency Domain - Tonal Noise of Rotors in Uniform Inflow," *4TU.ResearchData*, 2024. https://doi.org/10.4121/7da5aa45-e44b-4fa3-9407-8bf61e835d99.v1.

[29] Frey, F., Thiemeier, J., Öhrle, C., Keßler, M., and Krämer, E., "Aerodynamic Interactions on Airbus Helicopters' Compound Helicopter RACER in Cruise Flight," *Journal of the American Helicopter Society*, 2020. https://doi.org/10.4050/JAHS.65.042001.

[30] Kowarsch, U., Öhrle, C., Keßler, M., and Krämer, E., "Aeroacoustic Simulation of a Complete H145 Helicopter in Descent Flight," *Journal of the American Helicopter Society*, 2016. https://doi.org/10.4050/JAHS.61.042001.

[31] Richardson, L. F., "The Deferred Approach to the Limit," *Transactions of the Royal Society of London, Series A*, 1927.

[32] "Procedure for Estimation and Reporting of Uncertainty Due to Discretization in CFD Applications," *Journal of Fluids Engineering*, Vol. 130, 2008. https://doi.org/10.1115/1.2960953.

[33] Roache, P. J., "Perspective: A Method for Uniform Reporting of Grid Refinement Studies," *Journal of Fluids Engineering*, Vol. 116, 1994. https://doi.org/10.1115/1.2910291.

[34] de Vries, R., van Arnhem, N., Sinnige, T., Vos, R., and Veldhuis, L. L. M., "Aerodynamic interaction between propellers of a distributed-propulsion system in forward flight," *Aerospace Science and Technology*, Vol. 118, 2021. https://doi.org/10.1016/j.ast.2021.107009.

[35] Dürrwächter, L., Keßler, M., and Krämer, E., "Numerical Assessment of Open-Rotor Shielding with a Coupled Approach," *AIAA Journal*, 2019. https://doi.org/10.2514/1.J057531.